Available online at www.sciencedirect.com
SCIENCE DIRECT®
PERGAMON
International Journal of Heat and Mass Transfer 47 (2003) 111–124
International Journal of HEAT and MASS TRANSFER
www.elsevier.com/locate/ijhmt

Dendritic fins optimization for a coaxial two-stream heat exchanger

J. Bonjour [a,*], L.A.O. Rocha [b], A. Bejan [b], F. Meunier [a]

[a] Laboratoire du Froid (E.A. 21), CNAM, 292 rue Saint Martin, 75141 Paris Cedex 03, France
[b] Department of Mechanical Engineering and Materials Science, Duke University, Box 90300, Durham, NC 27708-0300, USA

Received 15 November 2002

Abstract

This paper documents the fundamental relation between the maximization of global performance and the maleable (morphing) architecture of a flow system with global constraints. The example is the coaxial two-stream heat exchanger with flow through a porous bed in the annular space. It is shown that the constraints force the design toward heat exchangers with finite axial length, where additional improvements are derived from installing high-conductivity fins across the porous bed. The maximization of global performance is achieved through the optimization of the configuration of plate fins. Configurations with radial fins are optimized analytically and numerically. Configurations with branched fins are optimized numerically. It is shown that the best configuration (radial vs. branched) depends on the size of the heat exchanger cross-section. When the size is small, the best is the radial pattern. When the size exceeds a certain threshold, the best configuration is the optimized branched tree of fins.

Keywords: Constructal design; Geometry optimization; Heat exchangers; Temperature swing adsorption; Fins; Tree networks

1. Introduction

In this paper we consider the fundamental problem of squeezing into a fixed volume the highest heat transfer rate that can be made to occur between two streams at different initial temperatures. This is a problem of great importance in the compaction and miniaturization of every flow system that requires heat exchangers. The approach that we have chosen is to allow the configuration of the heat exchanger to vary, and to select its architectural features such that the heat exchanger performs best at a global level. This work is an extension of the constructal design method [1], according to which the flow architecture of a system is free to vary and is deduced from a principle of global performance maximization subject to global constraints.

The coaxial heat exchanger selected for optimization in this paper is important because of its wide applicability: it is one of the simplest two-stream arrangements known [2,3]. In addition, it is a device that promises to play an important role in the development of efficient systems for temperature swing adsorption (TSA) [4–7]. This application served as stimulus for the present work, and for this reason we describe it in some detail.

Temperature swing adsorption processes are gas-separation processes based on a periodic variation of the temperature of an adsorbent porous bed. The adsorption occurs at a low temperature and the bed regeneration at a high temperature. TSA is usually recommended for purification (when a small fraction of the gas stream must be adsorbed, typically <10% by weight) rather than for bulk separation (high fractions) [8]. TSA cycle times are usually quite long (from several hours to several days) and are characterized by high energy consumption, which makes the cycle optimization (mass flow rates, temperature level, bed geometry) a subject of great importance.

* Corresponding author. Tel.: +33-1-58-80-85-51; fax: +33-1-40-27-25-95/20-47.
E-mail address: bonjour@cnam.fr (J. Bonjour).

0017-9310/$ - see front matter © 2003 Elsevier Ltd. All rights reserved.
doi:10.1016/S0017-9310(03)00406-X

Nomenclature

A	area, m^2
B	group of geometric parameters, m^3 K/W, Eq. (11)
c_p	specific heat at constant pressure, J/kg K
C_V	group of parameters that accounts for overall size, m^4, Eq. (24)
D_0	thickness of radial fin, m
D_1	thickness of peripheral (branched) fin, m
H	height, m
k	porous bed thermal conductivity, W/m K
k_f	fin thermal conductivity, W/m K
L	length, m
L_0	length of radial fin, m
L_1	length of peripheral (branched) fin, m
m	mass, kg
$\dot{m}$	mass flow rate, kg/s
n	number of heat exchangers
N	number of fins
q'''	heat transfer rate per unit volume, W/m^3
r	radial position, m
R	radius, m
$\widehat{R}$	dimensionless radius, Eq. (32)
u	volume averaged velocity, m/s
t	thickness, m
T	temperature, K
TSA	temperature swing adsorption
V	volume, m^3
V_f	fin volume, m^3
x, y	cartesian coordinates, m

Greek symbols

α	porous bed thermal diffusivity, m^2/s
β	angle, rad
ε	effectiveness
ρ	density, kg/m^3
ϕ	metal volume fraction

Subscripts

end	end of fin
f	fin
h	hot spot
in	inlet
min	minimal
out	outlet
s	shell
t	central tube

Superscript

$\tilde{()}$	dimensionless variables, Eqs. (30)

Most of the TSA processes use hot gas or steam for the regeneration phase. However, in the case of direct heating with steam, the adsorbent must be dried after the regeneration. In addition, if the adsorbate is miscible with water, a secondary unit must be used to separate the water. The hot gas technique leads to a diluted desorbed phase and, consequently, low condensation temperatures must be reached if the purpose of the process is to reuse the adsorbate. This is the reason why several alternative processes have been developed recently for the purpose of avoiding direct heating. These processes use Joule heating generated by the electrical resistance of the adsorbent [9], microwaves [10], thermoelectric devices [11], and indirect heating [12]. Indirect cooling and heating tend to shorten the cycle times, and this usually leads to higher energy performance [13].

TSA processes with indirect cooling and heating usually employ a column made of concentric tubes. The column is heated during the regeneration step and cooled during the adsorption step. The outer surface of the outer tube is insulated in order to reduce heat losses. Radial fins can be located on the outer surface of the inner tube, to enhance the global heat transfer coefficient and to decrease the nonuniformity in temperature and adsorbed-phase concentration. Short cycle times and high adsorption capacities require high global heat transfer coefficients during the heating and cooling periods. This recommends the use of a finned geometry on the porous bed side, where the heat transfer coefficients range from 10 to 50 W/m^2 K [14]. In addition, boiling or condensation inside the inner tube is preferable, because of high heat transfer coefficients: they range from 4000 to 7000 W/m^2 K, as measured in a simulated adsorption column by Mativet [15] and Mativet et al. [16].

Two main requirements drive the development of TSA technology: the need to reduce the adsorbent inventory, and the need to improve the overall process efficiently. Consequently, heat exchange optimization is a key issue because it reduces the regeneration time, improves the global effectiveness, and reduces the inert mass inventory.

In this paper, we explore the relationship between heat exchanger performance and the architecture of the fins that are distributed through the packed bed: radial fins vs. dendritic fins. In Sections 2 and 3 we begin with an analytical model of a coaxial heat exchanger with fins in the annular space. In Section 4 we include in the model the global constraints of fixed total volume and fin material, which points the design configuration in the direction of tubes of finite length, and annular spaces with embedded fins. The smallest construction detail is introduced as a manufacturing constraint in Section 5. Optimizations for fixed effectiveness and several heat exchangers in parallel are performed in Sections 6 and 7.

The optimization of cross-sectional configurations with radial and dendritic fins is pursued numerically in Section 8. The paper concludes with a design example, and a discussion of the role of dendritic flow structures in maximizing the global performance of heat exchangers.

2. Heat exchanger configuration

The objective of the following analysis is the optimization of the geometry of the two-stream heat exchanger shown in Fig. 1. One stream flows through a small-diameter tube placed on the centerline of a cylindrical shell of radius R and length L. The annular space is a packed bed through which the second stream flows axially. For simplicity, we assume that the tube on the centerline is isothermal and at the low temperature $T_{\min}$. This low temperature is maintained by a stream that evaporates as it flows at constant pressure through the tube.

The second stream is single-phase, and enters the annulus at the high temperature T_{in}. The flow rate, or the volume averaged axial velocity u is specified. The temperature of this stream drops while in contact with the $T_{\min}$ tube, and reaches its lowest temperature at the outlet, T_{out}. The effectiveness, or the total heat transfer rate between the two streams is maximal when T_{out} is minimal. To achieve this level of performance is the objective of the optimization of flow geometry, which is described next.

The geometry of the cylindrical structure is complicated by the installation of a number (N) of radial high-conductivity plate fins of thickness t. These serve two functions, to enhance the heat transfer between the two streams, and to provide rigidity for the assembly. In sum, the geometry of the device is represented by the parameters R, L, N and t. There are two global parameters that may serve as constraints in the optimization, the total volume of the heat exchanger,

$$V = \pi R^2 L \tag{1}$$

and the total volume of the fin material,

$$V_{\text{f}} = NtRL \tag{2}$$

The latter can also be represented by the volume fraction occupied by the fins,

$$\phi = \frac{V_{\text{f}}}{V} = \frac{Nt}{\pi R} \tag{3}$$

An alternative to the V_{f} constraint is the total mass of the heat exchanger,

$$m = (\rho_{\text{f}} NtR + \rho_{\text{s}} 2\pi R t_{\text{s}} + \rho_{\text{t}} A_{\text{t}})L \tag{4}$$

where ρ_{f}, ρ_{s}, t_{s}, ρ_{t} and A_{t} are the density of fin material, the density and thickness of the outer shell of radius R, and the density and cross-sectional area of the central tube.

3. Elemental volume

In this section we establish analytically the relationship between the global thermal conductance of the heat exchanger and the geometry of the apparatus. The model consists of the following steps:

First, we expect the fluid flow to be oriented practically in the axial direction, such that the velocity profile is as in plug flow. In this volume-averaged and time-averaged view of the packed bed, each streamline is parallel to the centerline. The flow does not feel the retarding effect of the solid walls.

Second, we assume that the axial temperature gradient ($\partial T/\partial x$) along a streamline (at fixed r and angular position β) is the same at every point in a $x =$ constant cross-section. This is an approximation that is more accurate downstream from the entrance, and when the flow length is long. In the present analysis, this assumption serves the following purpose: each streamline that pierces the $x =$ constant plane, deposits energy at the point of intersection at a uniform volumetric rate q''' [W/m^3],

$$q''' = \rho c_{\text{p}} u\left(-\frac{\partial T}{\partial x}\right) \tag{5}$$

where ρ and c_{p} are the fluid density and specific heat at constant pressure, and u is the volumetrically averaged velocity in the x direction. The flow distributes q''' uniformly over the disc of radius R. Later, this heat current

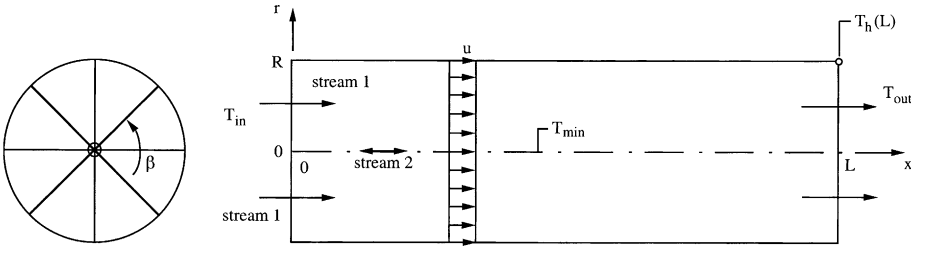

Fig. 1. Coaxial two-stream heat exchangers with radial plate fins.

finds its way to the heat sink (T_{min}) by first reaching the fins and flowing along them toward the center.

Third, thermal diffusion in the axial direction is neglected. The outer surface of the shell of radius R is insulated, and conduction along the shell in the angular direction is assumed negligible.

Fourth, we assume that the number of fins is sufficiently large that we may approximate the disc as a fan of N elemental wedges of the type shown in Fig. 2. This decomposition of the temperature field in a disc with uniform heat generation was used earlier in [17]. The element is an isosceles triangle of height R and base $2\pi R/N$. Heat is added at the rate q''' at every point (r, y). First, each heat current flows by thermal diffusion in the y direction through the packed bed. The effective thermal conductivity of the porous bed saturated with fluid is k. Later, the heat current makes a 90-degree turn, and flows along the nearest radial fin toward the center. The conductivity of the fin material is k_f.

By solving and matching the two thermal diffusion problems associated with the k and k_f materials, we obtain an approximate description of the temperature distribution over the elemental volume and the disc as a whole. The attractive feature of this result is that it expresses in closed form the relationship between the temperature field and the geometry of the element. The conduction along the plate fin is governed by the energy conservation equation

$$\frac{\mathrm{d}}{\mathrm{d}r}\left(k_f t \frac{\mathrm{d}T}{\mathrm{d}r}\right) + 2\frac{\pi r}{N} q''' = 0 \tag{6}$$

where the second term represents the rate of heat addition per unit of radial length. Note that $2\pi r/N$ is the total vertical length (in the k domain) over which the added heat current is integrated. By integrating Eq. (6) twice and invoking the boundary conditions $\mathrm{d}T/\mathrm{d}r = 0$ at $r = R$, and $T = T_{min}$ at $r = 0$, we obtain the temperature distribution along the fin,

$$T - T_{min} = \frac{\pi q'''}{N k_f t}\left(R^2 r - \frac{r^3}{3}\right) \tag{7}$$

The highest fin temperature is at the $r = R$ end, where $T = T_{end}$:

$$T_{end} - T_{min} = \frac{2\pi q''' R^3}{3 N k_f t} \tag{8}$$

The thermal diffusion in the y direction is driven by temperatures that are higher than the fin temperature. The highest temperature (T_h) occurs in the bed at $r = R$, in the two corners of the elemental triangle. The temperature variation in the y direction is parabolic, from T_h at $y = 2\pi R/(2N)$, where $\partial T/\partial y = 0$ (symmetry), to T_{end} at $y = 0$, where $\partial T/\partial y$ reaches its highest value. By solving the thermal diffusion problem with uniform heat addition between $y = 0$ and $y = 2\pi R/(2N)$ we obtain

$$T_h - T_{end} = \frac{q'''}{2k}\left(\frac{\pi R}{N}\right)^2 \tag{9}$$

Adding Eqs. (8) and (9) we find an estimate for the overall temperature difference over the element, which is the same as over the disc cross-section,

$$T_h(x) - T_{min} = q'''(x) B \tag{10}$$

In this expression, function B accounts for the element geometry,

$$B = \frac{\pi^2 R^2}{2kN^2} + \frac{2\pi R^3}{3 N k_f t} \tag{11}$$

The axial variation of the peak cross-sectional temperature, $T_h(x)$, is obtained by eliminating q''' between Eq. (11) and Eq. (5), in which $\partial T/\partial x = \partial T_h/\partial x$. Integrating

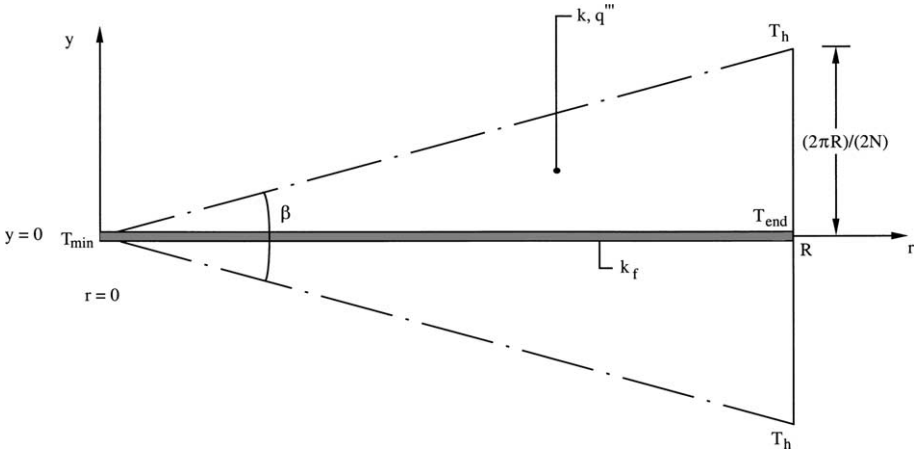

Fig. 2. Elemental volume centered around one plate fin.

the resulting equation starting from $T_h = T_{h,in}$ at $x = 0$, we find the exponential decay function

$$\frac{T_h(x) - T_{min}}{T_{h,in} - T_{min}} = \exp\left(-\frac{x}{\rho c_p u B}\right) \tag{12}$$

In particular, the highest temperature in the exit plane is $T_{h,out} = T_h(L)$,

$$\frac{T_{h,out} - T_{min}}{T_{h,in} - T_{min}} = \exp\left(-\frac{L}{\rho c_p u B}\right) \tag{13}$$

The dimensionless group formed on the left side is approximately the same as $1 - \varepsilon$, where ε is the effectiveness of the heat exchanger, because $T_{h,in} \cong T_{in}$ and $T_{h,out} \cong T_{out}$. This group decreases (the effectiveness increases) when the geometry-dependent group B/L decreases. This direction—the direction of smaller B/L values obtained through changes in geometry—is the direction explored in the next sections.

4. Fixed total volume and fin material

We orient our search for better geometries by starting with the volume constraint (1) and the associated fin material constraint (3). The length L can be eliminated from the B/L expression, and the result is

$$\frac{B}{L} = \frac{\pi R^4}{V}\left(\frac{\pi^2}{2kN^2} + \frac{2}{3k_f\phi}\right) \tag{14}$$

At constant V and ϕ, small B/L values are obtained when R is small and N is large. In view of Eq. (3), a small R also means a small Nt value. These two directions, small R and large N, are indicated in Fig. 3. If the fin thickness cannot be smaller than a certain value (t_{min}), which is dictated by mechanical strength requirements and the availability of fin plate material, then the $t = t_{min}$ constraint means

$$R \geqslant \frac{Nt_{min}}{\pi\phi} \tag{15}$$

This inequality limits the (R, N) domain only to the upper wedge shown in Fig. 3. The desirability of the smallest R and the largest N recommends the designs that fall on the straight dashed line, along which

$$N = \frac{\pi R\phi}{t_{min}} \tag{16}$$

Which end of this line is desirable, small (R, N) versus large (R, N), is indicated by the B/L expression (14), which after using Eq. (16) becomes

$$\frac{B}{L} = \frac{\pi}{V}\left(\frac{t_{min}^2 R^2}{2k\phi^2} + \frac{2R^4}{3k_f\phi}\right) \tag{17}$$

This expression shows that in order to obtain a small B/L we need to place the design in the limit $R \to 0$. Furthermore, because of the volume constraint (1), in the same limit we must have $L \to \infty$. In this limit, the heat exchanger is very long and narrow, and the fins are

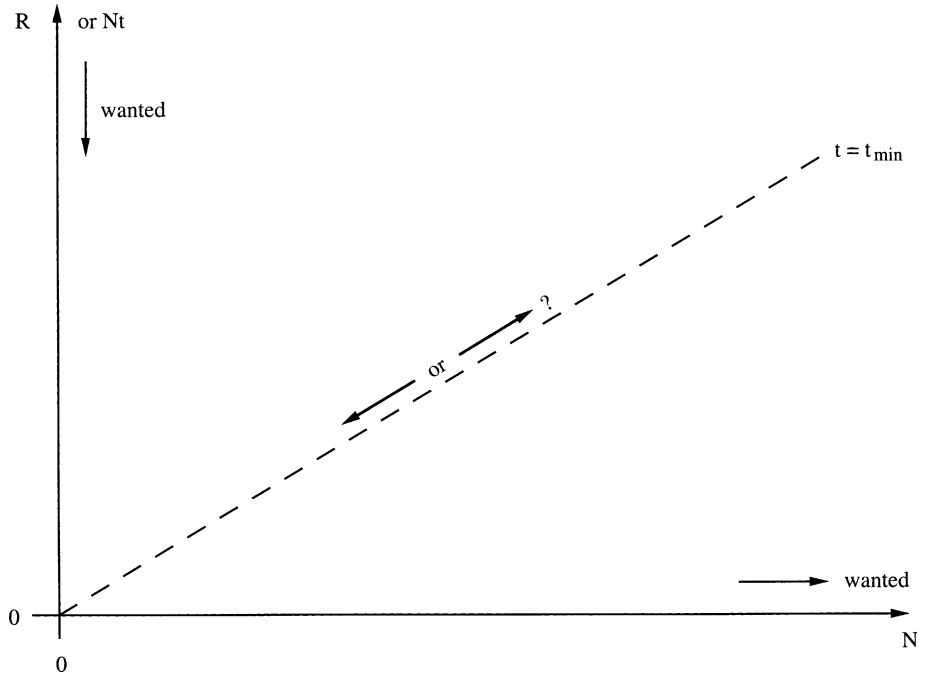

Fig. 3. Design space when the total volume and the volume of fin material are fixed.

absent. This limit is unrealistic because the $L \to \infty$ feature is prohibited by the pumping power requirement of operating the device. The power for pumping the fluid through the packed bed is proportional to L.

We reached the important conclusion that a device such as the heat exchanger of Fig. 1 must be a finite-length device. The finite length is another name for the pumping power constraint. Better thermal contact between the two streams must be achieved in ways other than stretching the device axially ad infinitum. The use of radial plate fins is one such method. The coaxial heat exchanger with radial plate fins emerges as an important (basic, necessary) configuration for a *finite-length heat exchanger*. This is the configuration on which we focus in the next section.

5. Fixing the smallest construction detail of the cross-section

In this section, we consider an important constraint in design, namely, the smallest structural detail that can be constructed. The cross-section geometry is accounted for by the B value, which should be small. If in Eq. (11) all the parameters are free to vary, then to minimize B means to minimize R, maximize N, and maximize t. This direction is not permissible, because it means that the entire cross-section is being filled by fin material.

If, in addition, we consider the fin volume fraction constraint (3), then the B expression becomes

$$B = \frac{\pi^2 R^2}{2kN^2} + \frac{2R^2}{3k_f\phi} \tag{18}$$

In this case, to achieve a small B means to use a small R and a large N, i.e., a progressively finer structure. This is the limit that brings to light the real-life constraint in the manufacturing of the cross-sectional design. The construction features cannot be smaller than a certain size. By construction features we mean not only the fin size (R) but also the distance ($2\pi R/N$) between two lines of attachment to the outer shell. This point of view is also consistent with the recognition of the smallest fin thickness constraint, $t = t_{\min}$, Eq. (15).

The constraint that covers the above ideas is the statement that the cross-sectional area of the elemental system of Fig. 2 is fixed,

$$A = \frac{\pi R^2}{N} \tag{19}$$

This area and the fin volume fraction ϕ are fixed, but the shape of the element [the ratio $(2\pi R/N)/R$, or N] is free to vary. The B function (11) assumes the form

$$B = \frac{A^2}{2kR^2} + \frac{2R^2}{3k_f\phi} \tag{20}$$

where the fin length R represents the lone degree of freedom. The B function reaches its minimum at

$$R_0 = \left(\frac{3k_f\phi}{4k}\right)^{1/4} A^{1/2} \tag{21}$$

which corresponds to

$$N_0 = \frac{\pi}{2}\left(3\phi\frac{k_f}{k}\right)^{1/2} \tag{22}$$

In conclusion, to maximize the thermal conductance of the A element means to select N, or to optimize the clustering of A-size channels into the radial arrangement chosen in Fig. 1. For example, if we use $k = 0.3$ $\mathrm{W\,m^{-1}\,K^{-1}}$ for the packed bed, $k_f = 60$ $\mathrm{W\,m^{-1}\,K^{-1}}$ for the fin material, and $\phi = 0.1$ for the fin volume fraction, then the optimal number of fins is $N_0 \cong 12$. The same number of fins was selected for the construction of a TSA column the thermal behavior of which was analyzed in [14]. Additional details on the column geometry and the performance of the TSA process are given in [18].

The optimized cluster also has a certain, deduced (not assumed) radial dimension, R_0. With L already fixed from pumping power requirements, this means that the size of the heat exchanger of the type shown in Fig. 1 is fixed. Larger sizes can be constructed by clustering more A-size elements, but this is possible only if the excess elements are arranged on the outside of the optimized central number, N_0. The fins of the external elements would have to be connected to the N_0 radial fins, and in this way the fin structure becomes a tree. This direction is illustrated in Fig. 4, and is explored later in Section 8.

6. Fixed effectiveness

An alternative is to approach the design from the point of view of the user who specifies a priori the desired values for effectiveness (ε), total volume (V), plate fin thickness (t), and volume averaged velocity (u). In this case the geometric unknowns are R, N, L and ϕ, however, as we show in this section, only one of these variables can serve as degree of freedom in the design.

The heat exchanger behavior is governed by Eqs. (1), (3), (13) and (18), with the observation that $(1-\varepsilon)$ can be written on the left side of Eq. (13). Note also that by using the general B expression (18), we free the design from the A constraint and optimization described in Section 5. Indeed, the approach described next is an alternative to the A-constrained optimization.

The analysis consists of two steps. First, we eliminate B between Eqs. (13) and (18), and then we use Eq. (1) to eliminate L. The result of combining Eqs. (1), (13) and (18) is a single equation

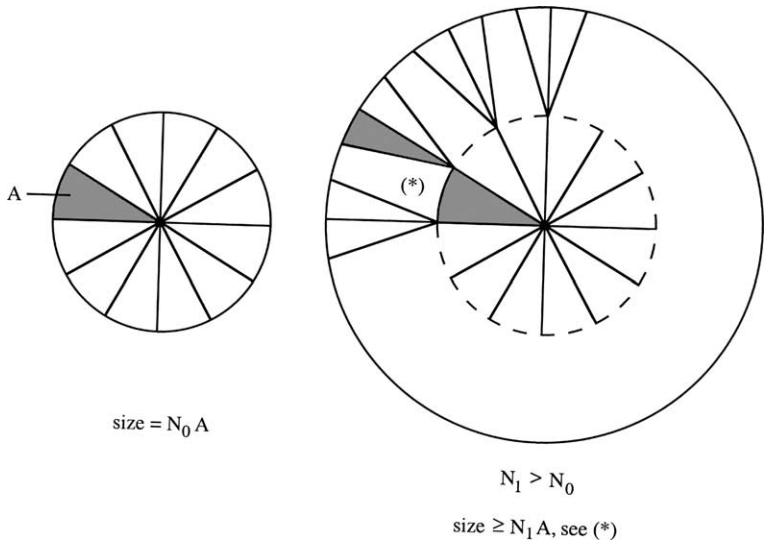

Fig. 4. The stepwise transition from a design with N_0 radial elements of size A, to a larger structure with branched elements of size A.

$$\frac{\pi^3 R^4}{2N^2} + \frac{2\pi^2 R^5}{3(k_f/k)Nt} = \frac{\alpha V}{u[-\ln(1-\varepsilon)]} \tag{23}$$

where $\alpha = k/(\rho c_p)$ is the equivalent thermal diffusivity of the porous bed as a fluid-saturated porous medium. Note that k is the thermal conductivity of the porous bed with the fluid in the pores, and ρc_p is the heat capacity of the fluid alone. Eq. (23) relates the specified data (V, ε, t, u) to two variables (R, N), while Eqs. (1) and (3) deliver the required (corresponding) values of L and ϕ.

In summary, Eq. (23) relates R to N, and this means that in this case the assumed radial geometry (Fig. 1) has only one degree of freedom, R or N. The term on the right side of Eq. (23) is a constant that rules the "scaling up" of the design. The geometric effect of increasing the overall size is not felt through V alone, rather, it is the special group of parameters C_V (V, ε, u, α), which accounts for increasing sizes:

$$C_V = \frac{\alpha V}{u[-\ln(1-\varepsilon)]} \tag{24}$$

The two terms on the left side of Eq. (23) have the same qualitative behavior with respect to R and N. Depending on which of the terms dominates, R is proportional to $N^{1/2}C_V^{1/4}$ or $(NtC_V)^{1/5}$. The radius depends weakly on the overall volume (C_V), and on the selected number of radial plate fins. To illustrate this behavior, in Fig. 5 we have plotted Eq. (23) for the case $V = 3.65$ dm^3, $\varepsilon = 0.9$, $u = 0.09$ m s^{-1} and $\alpha = 2.5 \times 10^{-4}$ m^2 s^{-1}, which is represented by $C_V = 440.3$ cm^4. We also assumed $t = 0.1$ cm, $k = 0.3$ W m^{-1} K^{-1} and $k_f = 60$ W m^{-1} K^{-1}. Fig. 5 confirms that R increases weakly with N. The corresponding solid volume fraction ϕ increases as R increases, indicating that weight considerations ($\phi \ll 1$) will limit the design freedom when R exceeds a certain order of magnitude. The figure also shows that the corresponding flow length (L) and the smallest area detail of the flow cross-section (A) decrease rapidly as R increases. The decreasing A stresses the importance of recognizing the manufacturing constraint (19), which was described in Section 5.

7. Several heat exchangers in parallel

Consider now the idea of increasing the performance of the process by using several heat exchangers in parallel. Fig. 6 shows three of the coaxial heat exchangers treated until now (Fig. 1). The total mass flow rate is fixed,

$$\dot{m} = n\pi R^2 \rho u \tag{25}$$

where n is the number of heat exchangers. The total volume is also fixed,

$$V = n\pi R^2 L \tag{26}$$

This volume constraint replaces Eq. (1). The objective continues to be the maximization of the effectiveness ε. Eq. (13) can be combined with Eqs. (25) and (26) to show that the quantity that must be maximized is

$$-\ln(1-\varepsilon) = \frac{V}{\dot{m} c_p B} \tag{27}$$

This expression shows that the number of parallel units has no effect on performance when $\dot{m}$ and V are fixed. The only route to increasing ε is by minimizing B. The design of the geometric configuration of the heat exchanger cross-section is all that matters. This finding stresses further the importance of the B minimization

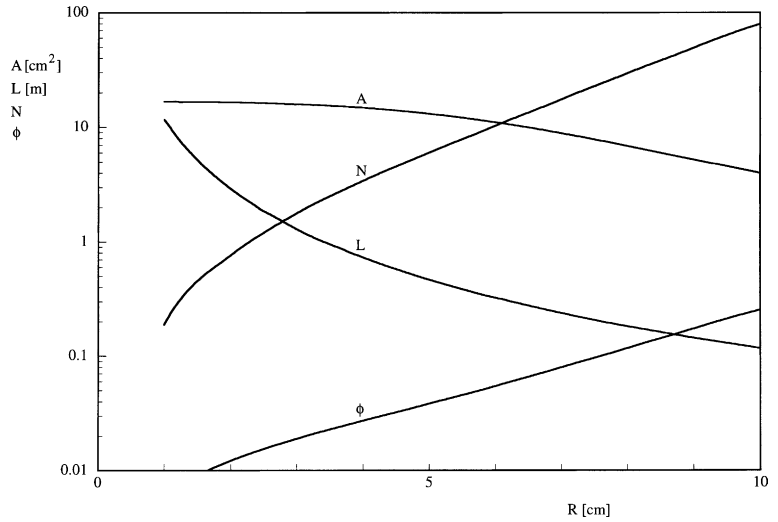

Fig. 5. Example of the relation between design features when the effectiveness, volume and volume-averaged fluid velocity (stream 1, Fig. 1) are fixed.

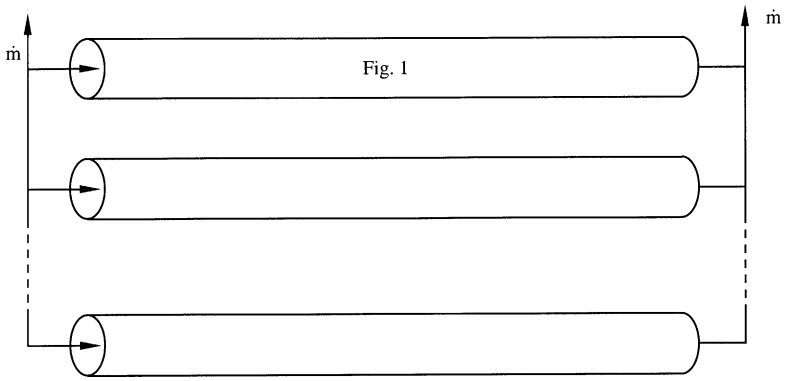

Fig. 6. The use of several heat exchangers in parallel.

method described in Section 5. We continue that approach in the next section.

8. Numerical optimization of the cross-sectional configuration

The numerical optimization of the cross-sectional configuration consisted of simulating the temperature field in many configurations, calculating the overall thermal resistance, and selecting the configuration that minimizes the thermal resistance. We started with the design with radial plate fins (Fig. 1), and assumed that the fins are numerous so that the cross-sectional area associated with one fin (A) is approximated by the triangle shown in Fig. 2. Symmetry allowed us to perform calculations in only half of the triangular A domain, Fig. 7. Heat deposition at the uniform rate q''', Eq. (5), occurs in the packed bed of conductivity k. The fin of half-thickness $t/2$ has the conductivity k_f, and no heat generation.

The conduction equations for points inside the k and k_f regions are, in order,

$$\frac{\partial^2 \widetilde{T}}{\partial \tilde{x}^2} + \frac{\partial^2 \widetilde{T}}{\partial \tilde{y}^2} + 1 = 0 \tag{28}$$

$$\frac{\partial^2 \widetilde{T}}{\partial \tilde{x}^2} + \frac{\partial^2 \widetilde{T}}{\partial \tilde{y}^2} = 0 \tag{29}$$

where the dimensionless variables are

$$(\tilde{x}, \tilde{y}, \widetilde{H}, \widetilde{R}, \tilde{t}) = \frac{(x, y, H, R, t)}{A^{1/2}} \quad \widetilde{T} = \frac{T - T_{\min}}{q''' A/k} \tag{30}$$

The three sides of the triangular $A/2$ domain are adiabatic. For the continuity of heat flux between the k and k_f regions (at $\tilde{y} = \tilde{t}/2$) we write

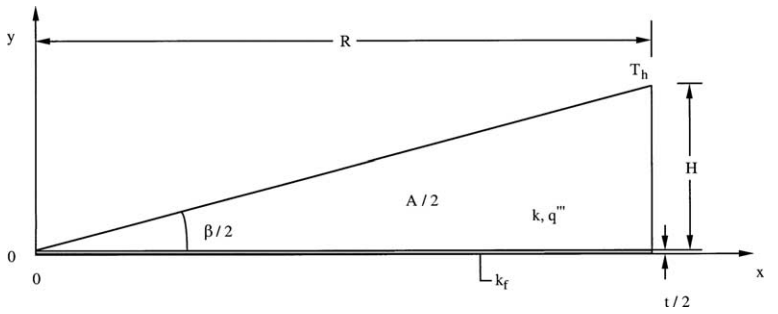

Fig. 7. Computational domain for the optimization of the design with radial plate fins.

$$\left(\frac{\partial \widetilde{T}}{\partial \tilde{y}}\right)_k = \frac{k_f}{k}\left(\frac{\partial \widetilde{T}}{\partial \tilde{y}}\right)_{k_f} \tag{31}$$

The highest temperature (T_h) always occurs in the corner that does not touch the fin. The dimensionless maximum temperature $\widetilde{T}_h$ represents the global thermal conductance of the $A/2$ domain, and of the entire disk shaped cross-section.

Eqs. (28) and (29) were solved using a finite element code [19]. We used quadrilateral elements with biquadratic interpolation functions. The grid was nonuniform in both $\tilde{x}$ and $\tilde{y}$, and varied from one geometry to the next. The appropriate mesh size was determined by successive refinements, until the further grid doubling of the number of grid points in both directions (N_x, N_y) met the criterion $|(\widetilde{T}_h^j - \widetilde{T}_h^{j+1})/\widetilde{T}_h^j| < 10^{-5}$. Here $\widetilde{T}_h^j$ represents the hot-spot temperature calculated using the current mesh size and $\widetilde{T}_h^{j+1}$ corresponds to the mesh where N_x and N_y were doubled. Table 1 gives an example of how grid independence was achieved. The results presented in this section were obtained by using $N_x = 129$ and $N_y = 97$. We further tested the accuracy of our finite element procedure by conducting similar calculations in a rectangular domain, and comparing the results with those published by Ledezma et al. [20]. The agreement between the two sets of results is within 0.02%.

We solved the conduction problem in many configurations ($\beta/2$, k_f/k, ϕ), where $\beta/2$ represents the shape of the $A/2$ triangle. We approximated $\beta/2 = \tan(H/R) \cong H/R$, which is consistent with the "many fins" assumption made at the start of this section—the assumption that one sector can be approximated by a triangle. Fig. 8 confirms that the thermal resistance can be minimized by selecting the shape of the triangular area, or the number of radial plate fins, $\beta/2 = \pi/N_0$. The shape optimized numerically is reported in Fig. 9, next to the analytical version of the same result, Eq. (22), or $\beta/2 = 2(3\phi k_f/k)^{-1/2}$. The lower part of Fig. 9 shows the corresponding results for the minimized thermal resistance, $\widetilde{T}_{h,min}$. Taking the numerical results as reference, we see that the analytical solution of Section 5 becomes more accurate as the group $\phi k_f/k$ increases.

Table 1
Numerical tests showing the achievement of grid independence ($\widetilde{H} = 0.4$, $\phi = 0.1$, and $k_f/k = 100$)

N_x	N_y	$\widetilde{T}_h$	$\lvert(T_h^j - T_h^{j+1})/T_h^j\rvert$
17	9	0.44600316	2.4585×10^{-4}
33	25	0.44591466	4.7430×10^{-5}
65	49	0.44589351	1.0406×10^{-5}
129	97	0.44588887	2.2425×10^{-6}
257	195	0.44588787	

The purpose of the numerical work on the radial fins configuration (Fig. 7) was to develop the numerical procedure, and to test it. This gave us the numerical capability of optimizing considerably more complicated configurations, such as the branched fins shown on the right side of Fig. 4. The first step in this direction is the optimization of the sector shown in Fig. 10, where each central fin has two branches, or more appropriately, two tributaries of heat flow by conduction. We fixed the area fraction occupied by fin material, $\phi = A_f/A$, where A_f is the area occupied by fin material ($A_f = L_0D_0 + 2L_1D_1$), and A is the total area of the sector ($A = 2H_1R$). The two-media composite is characterized by two parameters, and k_f/k, or ϕ and the group $\phi k_f/k$. We also fixed the smallest construction element, which is the area allocated to one of the small fins, $A_1 \cong L_1H_1$ when the total number of fins is sufficiently large. The heat flow configuration has three degrees of freedom: L_0/L_1, D_0/D_1 and

$$\widehat{R} = \frac{R}{A_1^{1/2}} \tag{32}$$

where unlike in the nondimensionalization used in Eqs. (30), $\widehat{R}$ is based on $A_1^{1/2}$ as length scale.

Heat conduction in the domain of Fig. 10 was simulated numerically by solving Eqs. (28)–(31), with the observation that A_1 replaces A in Eq. (30). The boundary conditions are adiabatic everywhere except at $x = y = 0$, where $\widetilde{T} = 0$. The temperature field was determined for a large number of configurations (D_0/D_1, L_0/L_1, $\widehat{R}$), and

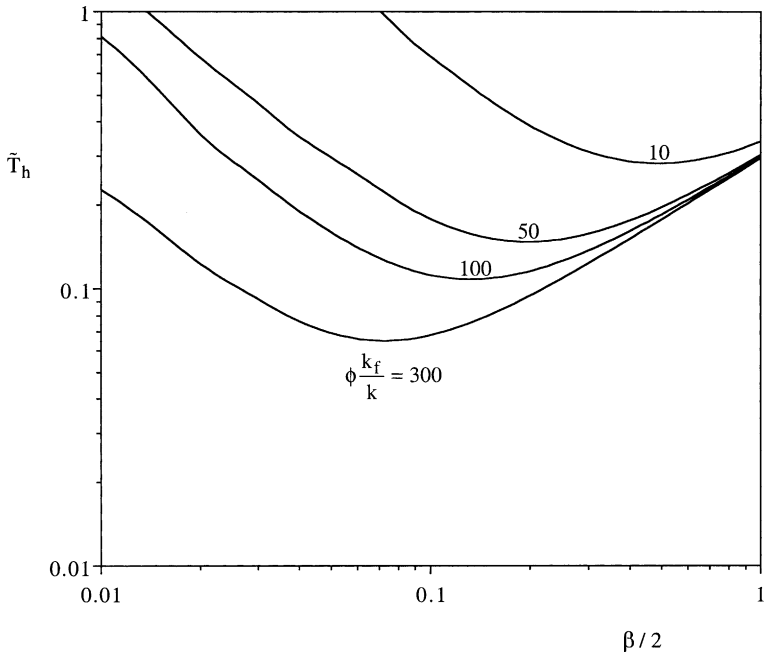

Fig. 8. The minimization of the overall thermal resistance in the element of Fig. 7.

in each case the hot-spot temperature $\widetilde{T}_h$ was recorded. The objective was to search for the configuration in which the overall thermal resistance $\widetilde{T}_h$ is minimum.

The search was conducted systematically, in three nested loops. The first and second loops consisted of varying D_0/D_1 and, respectively, L_0/L_1 in search of the $\widetilde{T}_h$ minimum. The D_0/D_1 and L_0/L_1 values were changed in steps of 0.1. To verify the validity of the results, the search was performed by varying L_0/L_1 first, and D_0/D_1 second, and the minimum was found to be the same as in Fig. 11. The parameter $\phi k_f/k$ was set equal to 30, because this represents the order of magnitude that corresponds to the values used in the experimental examples cited earlier in the paper.

The third loop consisted of varying $\widehat{R}$. Fig. 11 shows how the optimal results respond to changes in $\widehat{R}$. The ratios $(D_0/D_1)_{opt}$ and $(L_0/L_1)_{opt}$ reach a plateau when $\widehat{R}$ becomes greater than approximately 10. Another interesting feature is the "transition" found at $\widehat{R} \cong 4$. When $\widehat{R}$ is smaller than this critical value, the designs with purely radial fins are better than the optimized designs with branched fins. The minimized overall thermal resistance $\widetilde{T}_{h,min}$ decreases smoothly as $\widehat{R}$ crosses the $\widehat{R} \cong 4$ transition.

9. Design example

Future work may focus on the use of the methodology of this paper in design. Here we present one example. Consider the sizing of an actual adsorption column for a TSA process. The column is made of n smaller columns (called "units", e.g., Fig. 1), which are assembled into a "package", as shown in Fig. 12. The following assumptions serve as constraints:

(a) The volume of activated carbon that fills all the units is fixed at $V = 4\ m^3$, because it is dictated by the objectives of the TSA process. This volume corresponds to a weight of 2 tons, which is a typical size used in industry.
(b) The plate fins are made of copper ($k_f = 400$ W/m K) with a thickness of 1 mm.
(c) The heat exchanger effectiveness is 0.9.
(d) The fluid velocity is fixed at 0.09 m/s.
(e) The length of the unit should not exceed 5 m, and, in addition, the length/diameter ratio of each unit should be approximately 5, which is the usual aspect ratio in adsorption columns.
(f) The other physical parameters are assumed to have the same values as in the example given at the end of Section 6.

According to the conclusion of Section 7, to optimize the package of n columns means to optimize a single unit, the volume of which is $V_n = V/n$. Table 2 presents the main characteristics of the package and the units. These depend on the number of units, the necessary unit diameter, length and aspect ratio, and also on the number of fins in each unit and the solid volume fraction ϕ.

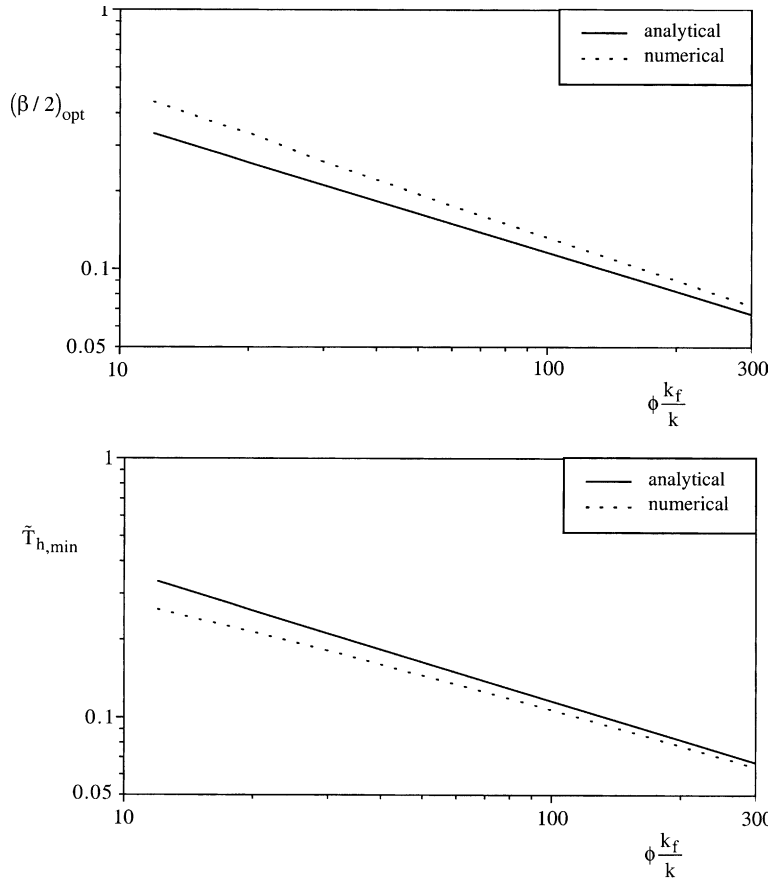

Fig. 9. The optimized shape of the element of Fig. 7, and the minimized thermal resistance.

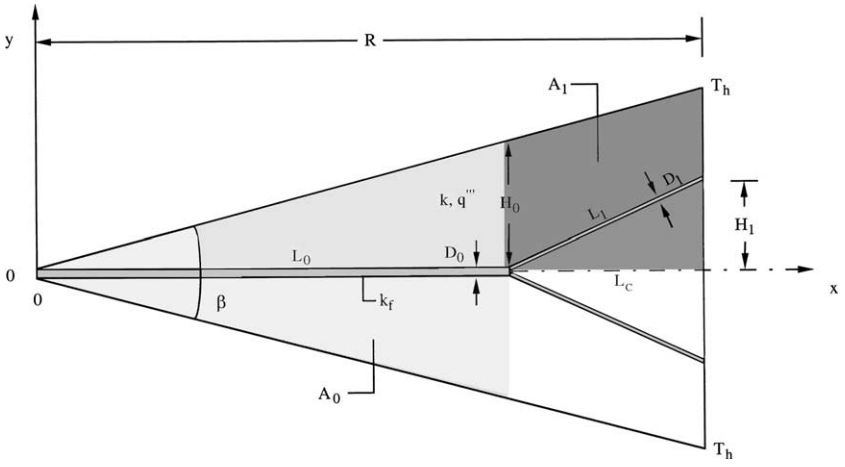

Fig. 10. Computational domain for the optimization of the design with branched plate fins.

For the total package, Table 2 shows the total metal volume, aspect ratio, mass of metallic fins, mass of the metallic jackets of the units, and the total mass (fins and jackets). The fin density is 8900 kg/m^3 (copper), and that of the jacket is 7800 kg/m^3 (stainless steel of thickness 2 mm). The fluid is air, with $k = 0.3$ W/m K. The copper

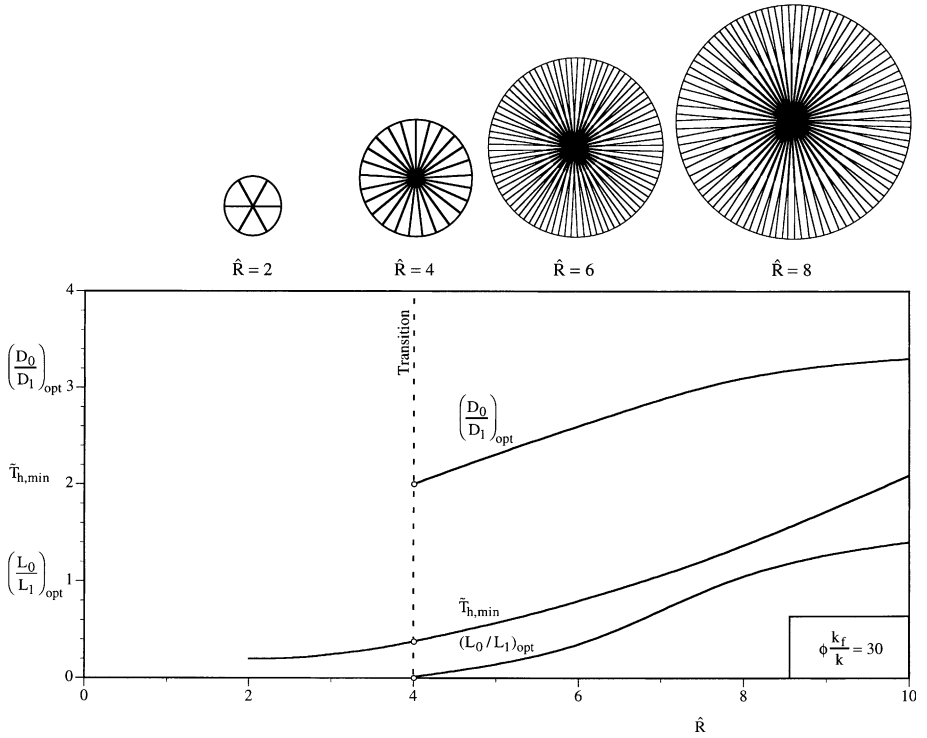

Fig. 11. The effect of the overall size ($\widehat{R}$) on the optimized architecture and performance determined numerically.

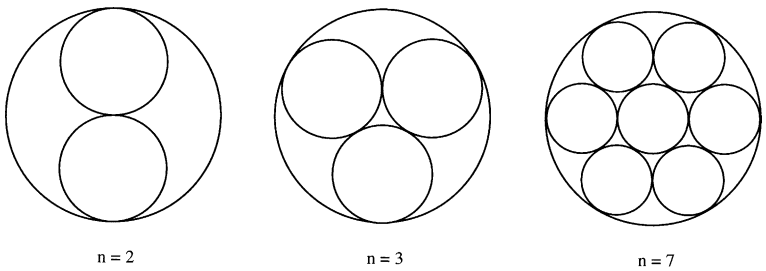

Fig. 12. Arrangement of n units into a package.

Table 2
The main characteristics of packages and corresponding units in Fig. 12

n	R (m)	L (m)	N	ϕ	V_{pack} (m^3)	$\widehat{R}$	m_{fins} (kg)	m_{jackets} (kg)	m_{total} (kg)
1	0.5	5	40	0.0237	4	5.83	843.7	39.0	882.7
2	0.4	4	27	0.0215	8	4.25	765.4	50.0	815.4
3	0.35	3.5	22	0.0205	6.33	2.65	729.8	57.4	787.2
4	0.317	3.17	19	0.0198	5.84	2.46	704.9	62.8	767.7
7	0.26	2.6	15	0.0191	5.05	2.18	680.0	74.0	754.0
14	0.209	2.09	12	0.0188	5.02	1.95	669.3	95.6	764.9

conductivity is $k_{\text{f}} = 400$ W/m K. The group $\phi k_{\text{f}}/k$ varies from 32 to 25, hence the representative value ($\phi k_{\text{f}}/k = 30$) used in Fig. 11.

When $n = 1$, the package consists of a single unit the volume of which is that of the adsorbent, but it requires an unreasonably large number of fins ($N = 40$). In-

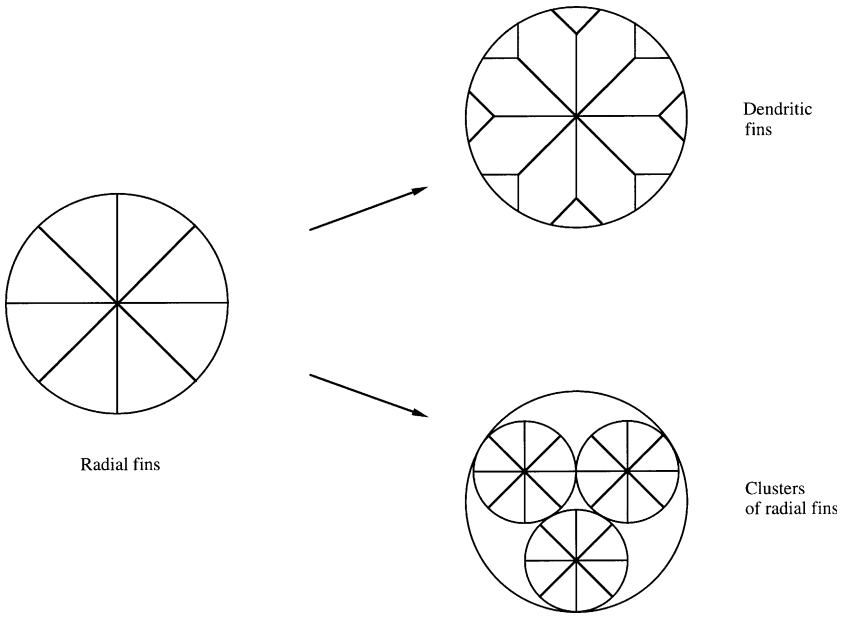

Fig. 13. Three competing configurations in the design of fins for coaxial heat exchangers.

creasing the number of units allows us to reduce the unit radius and length, together with the number of fins. *A* reasonable number of fins (10–20) thus corresponds to a package of 4–14 units.

The package volume is maximum when $n = 2$, because in this case half of the package does not actually contain adsorbent (Fig. 12). The package volume decreases slightly when more units are used. The mass of metallic fins decreases when n increases, because the metal volume fraction and the number of fins per unit decrease. At the same time, the mass of the jackets increases. These conflicting trends are the reason for the minimum in the total mass, which appears in the vicinity of $n = 7$. This number can be selected if it yields a reasonable number of fins and the minimization of the metal mass. This choice is illustrated by the lower arrow in Fig. 13.

A choice can also be made between designs with radial fins and designs with branched fins. Indeed, the $\widehat{R}$ values of the configurations proposed in Table 2 indicate that if packages are made of one or two units, then the branched fins would be preferable to radial fins when $\widehat{R} \gtrsim 4$ (cf. Fig. 11, and the first two cases in Table 2). See also the upper arrow in Fig. 13.

10. Summary and conclusions

In this paper we considered the fundamental connection between heat exchanger architecture and the maximization of global heat exchanger performance under global constraints. The two-stream coaxial heat exchanger was chosen because of its simplicity and the modern applications reviewed in Section 1. We showed that the constraints push the design toward that of a heat exchanger of finite length. Performance can be improved further by inserting high-conductivity plate fins in the porous bed.

The method of optimization was applied to the sizing of adsorption columns for TSA processes. Although it was shown that the method is applicable, it must be stressed that because of the cyclical nature of such processes (alternating periods of fast and slow flow, for adsorption and desorption, respectively) the column design cannot be optimized for both periods. If the optimization is performed for high velocities, then the column is over-sized for desorption operation, which means that it will have more fins than necessary for desorption. On the other hand, optimizing the column for desorption means that the performance will be low during adsorption.

The chief conclusion of this study is that it is possible to optimize the configuration of the plate fins so that the global thermal resistance of the heat exchanger is minimized. Radial fins and dendritic fins compete for maximal global performance. The optimal configuration depends on the size of the heat exchanger cross-section (radius R), relative to the length scale of the smallest fin structure that can be manufactured (length scale $A_1^{1/2}$). From a practical standpoint, this is the first study that recommends the use of tree-shaped fins in industrial-scale heat exchangers designed for maximal heat transfer density.

References

[1] A. Bejan, Shape and Structure, from Engineering to Nature, Cambridge University Press, Cambridge, UK, 2000.
[2] S. Kakac, A.E. Bergles, F. Mayinger (Eds.), Heat Exchangers: Thermal-Hydraulic Fundamentals and Design, Hemisphere, Washington, DC, 1981.
[3] R.K. Shah, A.C. Mueller, Heat exchangers, in: W.M. Rohsenow, J.P. Hartnett, E. Ganic (Eds.), Handbook of Heat Transfer Applications, 2nd ed., McGraw-Hill, New York, 1985 (Chapter 4).
[4] F. Meunier, Adsorption for environment, in: 7th Conf. Fundamentals of Adsorption (FOA7), Nagasaki, Japan, May 20–25, 2001.
[5] R. Kumar, M. Huggahalli, S. Deng, M. Andrecovitch, Trance impurity removal from air, in: Annual AIChE Meeting, Los Angeles, CA, November 12–17, 2000.
[6] J.J. Nowobilski, Perforated plate fluid distributor and its associated fixed bed vessel, US Patent No. 5,298,226, March 29, 1994.
[7] J.J. Nowobilski, J.S. Schneider, Particle loader, US Patent No. 5,324,159, June 28, 1994.
[8] G.E. Keller, Gas-adsorption processes: state of the art, in: Industrial Gas Separations, ACS Symp. Ser. 223, 1983.
[9] M. Baudu, P. Le Cloirec, G. Martin, Thermal regeneration by Joule effect of activated carbon used for air treatment, Environ. Technol. 13 (1992) 423–435.
[10] E.J. Mezey, S.T. Dinovo, Adsorbent regeneration and gas separation utilizing microwave heating, US Patent No. 4,322,394, 12 August 1980.
[11] M. Bonnissel, L. Luo, D. Tondeur, Fast thermal swing adsorption using thermoelectric devices and new adsorbent, in: F. Meunier (Ed.), Proceedings of the 6th Conf. Fundamentals of Adsorption (FOA6), Elsevier, Paris, 1998, pp. 1065–1070.
[12] A. Salden, T. Boger, G. Eigenberger, A combined vacuum and temperature swing adsorption process for the removal and recovery of organic components from waste-air-systems, in: F. Meunier (Ed.), Proceedings of the 6th Conf. Fundamentals of Adsorption (FOA6), Elsevier, Paris, 1998, pp. 915–920.
[13] M.M. Davis, M.D. LeVan, Experiments on optimization of thermal swing adsorption, Ind. Eng. Chem. Res. 28 (1989) 778–785.
[14] J. Bonjour, A. Mativet, J.B. Chalfen, F. Meunier, Identification du coefficient de transfert de chaleur par convection à travers un milieu poreux, 3èmes Journées Tunisiennes sur les Ecoulement et les Transferts, Mahdia, Tunisia, November 2000.
[15] A. Mativet, Etude Expérimentale d'un procédé de chaffauge et de refroidissement par changement de phase du fluide caloporteur, Doctoral Thesis, Univ. Paris XI, 1997.
[16] A. Mativet, F. Meunier, J.B. Chalfen, C. Marvillet, Experimental study of heat transfer during film condensation in transient conditions in a vertical smooth tube, Exp. Heat Transfer 12 (1999) 247–263.
[17] L.A.O. Rocha, S. Lorente, A. Bejan, Constructal design for cooling a disc-shaped area by conduction, Int. J. Heat Mass Transfer 45 (2002) 1643–1652.
[18] J. Bonjour, J.B. Chalfen, F. Meunier, Temperature swing adsorption process with indirect heating and cooling, Ind. Eng. Chem. Res. 41 (23) (2002) 5802–5811.
[19] FIDAP, Theory Manual, Vol. 7.0, Fluid Dynamics International, Evanston, IL, 1993.
[20] G.A. Ledezma, A. Bejan, M.R. Errera, Constructal tree networks for heat transfer, J. Appl. Phys. 82 (1997) 89–100.